Protected Amino Acid-Based Hydrogels Incorporating Carbon Nanomaterials for Near-Infrared Irradiation-Triggered Drug Release

Chloé Guilbaud-Chéreau, Bhimareddy Dinesh, Rachel Schurhammer, Dominique Collin, Alberto Bianco, Cécilia Ménard-Moyon

Protected Amino Acid-Based Hydrogels Incorporating Carbon Nanomaterials for Near-Infrared Irradiation-Triggered Drug Release

Chloé Guilbaud-Chéreau,[†] Bhimareddy Dinesh,[†] Rachel Schurhammer,[‡] Dominique Collin,[§] Alberto Bianco,*[,†] and Cécilia Ménard-Moyon*[,†]

[†]University of Strasbourg, CNRS, Immunology, Immunopathology and Therapeutic Chemistry, UPR 3572, 67000 Strasbourg, France

[‡]Laboratoire de Chimie moléculaire de l'état solide (UMR 7140 CNRS), Université de Strasbourg, 1 rue Blaise Pascal, 67081 Strasbourg, France

[§]Institut Charles Sadron, Université de Strasbourg, 23 rue du Loess, BP 84047, 67034 Strasbourg Cedex, France

Keywords: carbon nanotubes, graphene oxide, rheology, self-assembly, therapy

Abstract

Molecular gels formed by self-assembly of low molecular weight gelators have received increasing interest due to their potential applications in drug delivery. In particular, the ability of peptides and amino acids to spontaneously self-assemble into three-dimensional fibrous network has been exploited in the development of hydrogels. In this context, we have investigated the capacity of binary mixtures of aromatic amino acid derivatives to form hydrogels. Carbon nanomaterials, namely oxidized carbon nanotubes or graphene oxide, were incorporated in the two most stable hydrogels, formed by Fmoc-Tyr-OH/Fmoc-Tyr(Bzl)-OH and Fmoc-Phe-OH/Fmoc-Tyr(Bzl)-OH, respectively. The structural and physical properties of these gels were assessed using microscopic techniques and rheology. Circular dichroism and molecular dynamics simulations demonstrated that the hydrogel formation was mainly driven by aromatic interactions. Finally, a model hydrophilic drug (L-ascorbic acid) was loaded into the hybrid hydrogels at high concentration. Under near-infrared light irradiation a high amount of drug was released triggered by the heat generated by the carbon nanomaterials, thus offering interesting perspectives for controlled drug delivery.

1. Introduction

Self-assembled structures have gained great attention for the design of hydrogels and gel-like materials due to their wide range of applications going from controlled drug delivery and tissue engineering to nanoelectronics.[1-5] Supramolecular gels formed by the self-assembly of low molecular weight gelators (LMWGs) are receiving significant attention thanks to their potential in the biological field,[6] for instance in drug delivery.[7] These LMWGs self-assemble in water *via* non-covalent forces such as hydrogen bonding, hydrophobic interactions, and π-stacking.[8] These interactions lead to the formation of three-dimensional fiber-like networks and soft-solid-like materials by fiber entanglement, restriction of the solvent flow and trapping of the solvent molecules, resulting in hydrogel formation. LMWG-based gels possess advantages such as easy preparation and multiple responsiveness, compared to polymer gels, where the monomers are covalently bonded. Indeed, they can be responsive to different stimuli including pH and temperature.[9] Some peptides and amino acids having the capacity to self-assemble into fibrils have been exploited as LMWGs.[10-13] These types of hydrogels have shown potential applications in drug delivery,[14,15] tissue engineering,[16] and regenerative medicine.[17] Peptides and amino acids protected at the N-terminus with aromatic groups such as pyrene, naphthalene, and fluorenylmethoxycarbonyl (Fmoc) have been investigated as LMWGs.[18-21] Hybrid hydrogels incorporating carbon-based nanomaterials, such as carbon nanotubes (CNTs) and graphene, have recently attracted increasing attention due to their high electrical conductivity and high mechanical strength.[22-26] In addition, these hybrid hydrogels are useful for near-infrared (NIR) irradiation-triggered drug release, thanks to the capacity of the carbon nanomaterials to generate heat upon NIR light irradiation.[27-31] This feature is advantageous for on-demand drug release because light can be used as an external stimulus to control the liberation of active molecules preloaded in the hybrid hydrogels due to enhanced local temperature, with high spatial and temporal precision. In addition, NIR light is more favorable than visible light for *in vivo* applications due to its higher penetration, low energy absorption, and minimum side effects for human tissue and organs. Both GO and functionalized CNTs have been extensively used for biomedical applications.[32,33] We and other groups have previously demonstrated the absence of toxicity of well-purified and functionalized CNTs[34-36] and GO[37,38] *in vitro* and *in vivo*. The choice of carbon-based nanomaterials as photothermal agents among others such as gold nanoparticles, was mainly dictated by the possibility to tune their biodistribution and biodegradation, and to minimize toxicity through size control and chemical functionalization. Indeed, several studies have demonstrated that both CNTs and GO can be easily biodegraded under biological conditions hence sensibly reducing their biopersistence,[39-

[41] while studies on the biodegradability of gold nanoparticles are scarce. Both GO and functionalized CNTs have been widely used as photothermal agents.[42] In this work, we have screened a variety of aromatic amino acid derivatives for their capacity to form hydrogels. Oxidized CNTs (ox-CNTs) or graphene oxide (GO) were incorporated into two stable hydrogels, made of Fmoc-Tyr-OH/Fmoc-Tyr(Bzl)-OH and Fmoc-Phe-OH/Fmoc-Tyr(Bzl)-OH. The hybrid hydrogels were characterized by different techniques including electron microscopy, circular dichroism (CD), and rheology. Molecular dynamics (MD) simulations were performed to understand the main interactions leading to the formation of the hydrogels. Finally, L-ascorbic acid was incorporated in the hybrid hydrogels as model drug. A high amount of drug was released upon NIR light irradiation, thus offering interesting perspectives for drug release that can be precisely and remotely controlled through external stimuli.

2. Results and discussion

2.1. Hydrogel formation

Different single and binary mixtures of protected and non-protected aromatic amino acids were initially studied for hydrogelation (Figure S1). The samples were prepared using the solvent-triggered approach where the gelators are first dissolved in DMSO by using sonication followed by addition of water to reach 2% DMSO/H_2O (v/v).[43] At such low concentration DMSO can be used in biological experiments as it shows no cytotoxicity.[44,45] We observed that binary systems composed of non-protected amino acids were highly soluble leading to optically transparent solutions, whereas co-assemblies of protected amino acids resulted in the formation of precipitates in biphasic systems made of gel and liquid, or led to gel-like structures (Table S1). The gelation of the samples was confirmed by the vial inversion test and we observed that 14 mixtures formed a hydrogel. In all cases at least one of the components was a Fmoc-protected amino acid derivative. Our results confirm that the presence of the aromatic fluorenyl ring helps in the gelation process.[4,20,46,47] Most hydrogels were obtained from a binary mixture containing Fmoc-Tyr-OH or Fmoc-Tyr(Bzl)-OH. For this reason, we decided to focus our comparative work on two stable hydrogels corresponding to the binary systems Fmoc-Tyr-OH/Fmoc-Tyr(Bzl)-OH (named gel 1) and Fmoc-Phe-OH/Fmoc-Tyr(Bzl)-OH (named gel 2) (Figure 1). We noticed that a sequential addition of DMSO and water was very important as the dissolution of the gelators directly in a mixture of 2% DMSO in water did not result in gel formation.

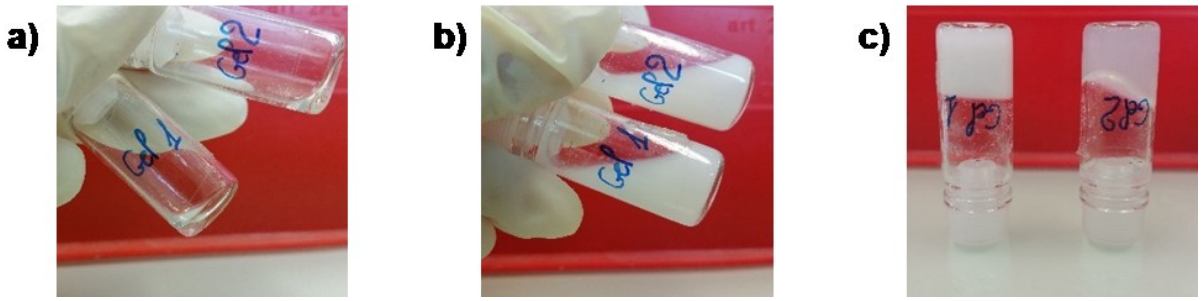

Figure 1. Photographs of the formation of gel 1 and gel 2: a) solution of the amino acids in DMSO, b) immediately after the addition of water, and c) after 2 h.

2.2. Formation of hydrogels containing carbon nanomaterials

Since carbon nanomaterials have excellent photothermal properties under NIR light irradiation, hybrid hydrogels containing CNTs or graphene offer a great potential for NIR irradiation-triggered drug release applications. We first studied the incorporation of pristine CNTs and ox-CNTs at three different concentrations (0.025 wt%, 0.1 wt% and 0.5 wt%) into gel 1. For this purpose, aqueous suspensions of pristine CNTs or ox-CNTs were prepared by sonication and immediately added to the solution of gelators in DMSO. The gelation time was not affected by the presence of the pristine CNTs. However, due to their low water dispersibility, the pristine CNTs were non-homogenously dispersed in the gel at all concentrations obtaining heterogeneous gels (Figure S2a-c). But, the dispersion was drastically improved by using ox-CNTs and we observed that the maximum concentration of ox-CNTs that can be incorporated into gel 1 to obtain a homogeneous hybrid gel was 0.025 wt% (Figure S2d). Increasing the concentration of nanomaterials disturbed the gelation process as we observed the appearance of a liquid phase (Figure S2e-f). Therefore, 0.025 wt% was chosen as the optimal concentration of ox-CNTs. The same experiments were performed using 0.025 wt% of GO instead of ox-CNTs to compare the gelation behavior (Figure 2). GO is known to have a superior water dispersibility than graphene. The incorporation of GO did not prevent the gel formation. We noticed that the gel color was more homogeneous for gel 2 compared to gel 1, whatever ox-CNTs or GO had been incorporated into the gel. This difference indicates that gel 2 seems to be more homogeneous compared to gel 1.

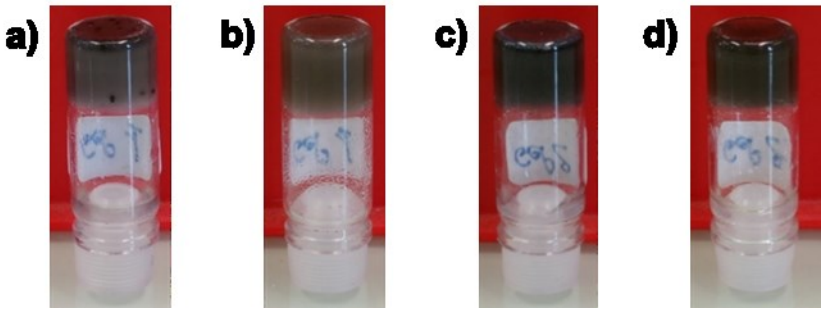

Figure 2. Photographs of a) gel 1 + 0.025 wt% ox-CNTs, b) gel 1 + 0.025 wt% GO, c) gel 2 + 0.025 wt% ox-CNTs, and d) gel 2 + 0.025 wt% GO, after 2 h gelation.

2.3. Structural characterization

The morphology of native and hybrid gel 1 and gel 2 was studied by scanning electron microscopy (SEM) and transmission electron microscopy (TEM). The SEM images of the native gels show the presence of long fibrils organized into highly interconnected networks (Figure 3a-b). The TEM analysis revealed that the majority of the fibrils in gel 1 (Figure 3c) has a width of 10-50 nm with a few larger fibrils (50-80 nm) (Figure S3a). In the case of gel 2 (Figure 3d), although the majority has a width of 20-50 nm similar to gel 1, the fibrils are more variable in size having a diameter in the range of 20-100 nm (Figure S3b). This difference suggests that the presence of the hydroxyl group of tyrosine can influence the fibril width probably due to the formation of additional hydrogen bonding. The presence of ox-CNTs does not disturb the self-assembly of the amino acid derivatives into fibrils of similar size and morphology (Figure 3e-f, Figure S3c-d), but we observed a higher diameter distribution for both gels containing GO from 10 to 200 nm (Figure 3g-h, Figure S3e-f). The TEM images also show that the ox-CNTs and GO are in contact with the fibrils certainly due to π-π interactions with the aromatic moieties of the gelators (Figure 3e-h). Especially, the ox-CNTs are in close interactions with the surface of the fibrils, which may be facilitated by their tubular shape. In Figure 3f-h, we selected images showing a lower fibril density in order to be able to visualize the carbon nanomaterials and their interactions with the fibrils. This is the reason why the fibrils look less aggregated.

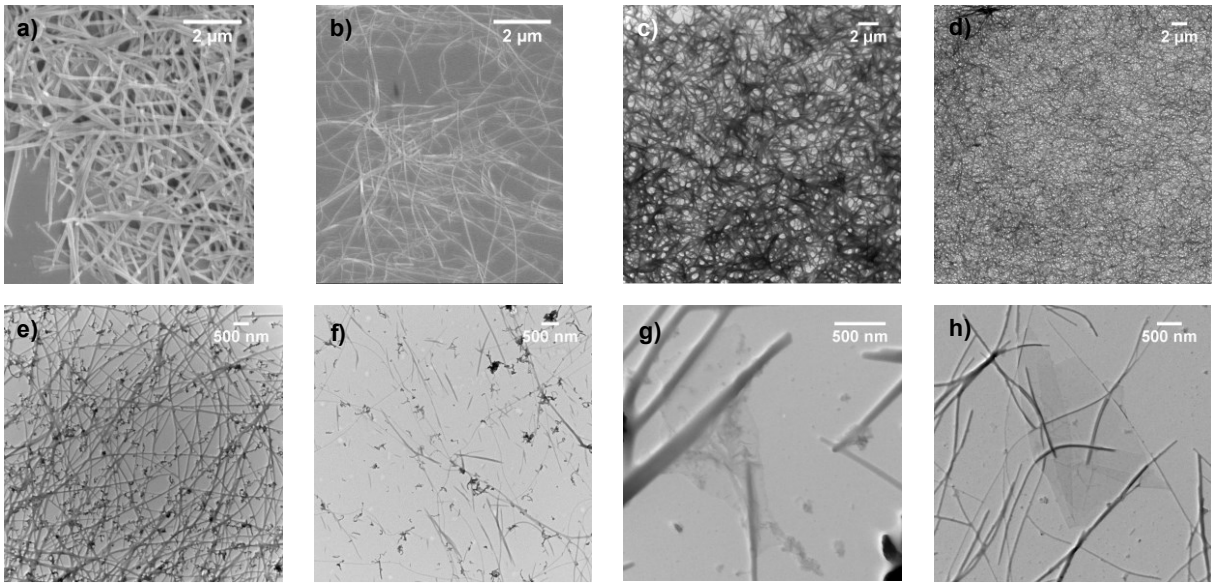

Figure 3. SEM images of a) gel 1 and b) gel 2. TEM images of c) gel 1, d) gel 2, e) gel 1 + 0.025 wt% ox-CNTs, f) gel 2 + 0.025 wt% ox-CNTs, g) gel 1 + 0.025 wt% GO, and h) gel 2 + 0.025 wt% GO.

2.4. Circular dichroism

The native gel 1 and gel 2 and the hybrid gels containing the nanomaterials were characterized by CD. Previous studies have shown that fibrils derived from Fmoc aromatic amino acids are supported by π–π interactions between aromatic moieties, with characteristic CD signatures at 270-310 nm attributed to the n–π* Fmoc-Fmoc transition and at 200-230 nm corresponding to the π–π* phenyl side chain transition, and a hydrogen bond network involving the carbamate functionality.[48] For all samples the gel solutions were sonicated 10 s before being transferred into a cylindrical 0.1 mm quartz cuvette. The kinetics of the hydrogelation process was studied by monitoring the CD signal as a function of time. The CD spectrum of gel 1 does not show any signal at t0 (Figure 4a). After 1 h the hydrogelation was characterized by the appearance of a negative band centred at ~220 nm and a broad positive band between 270 and 310 nm. These two bands are derived from the π-π amino acid side chain-side-chain and Fmoc-Fmoc interactions.[49] An increase of the signal was observed between 1 h and 2 h showing that the co-assembly can be described as a two-step mechanism, a first step of fibril organization into chiral structures and a second step of evolution of the final fibrils to an equilibrium state. The CD analysis was performed for longer time (> 2 h), but no significant differences were observed compared to the spectrum at 2 h (data not shown), indicating that the three-dimensional fibrous network reached a steady state.

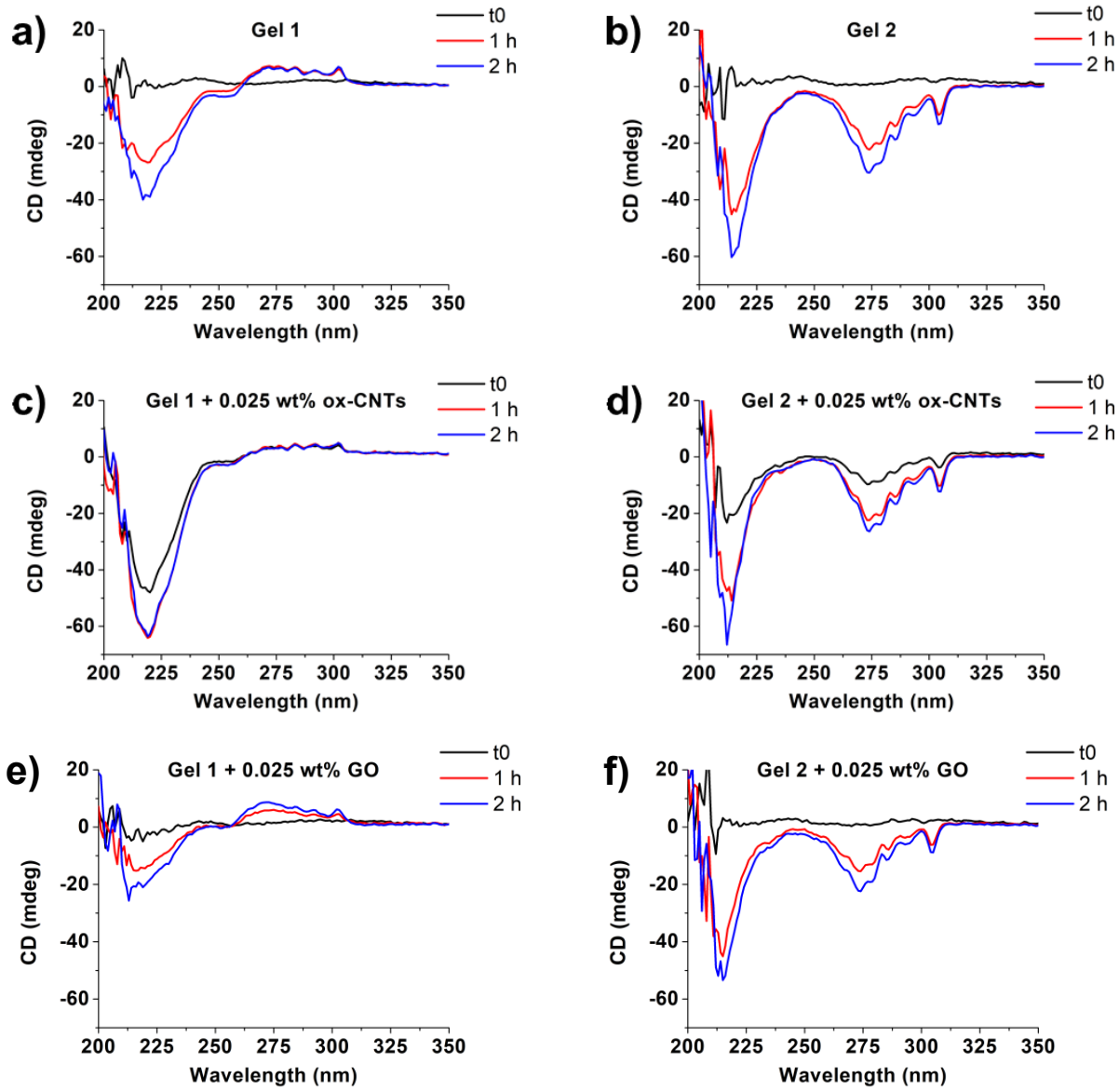

Figure 4. CD spectra of a) gel 1, b) gel 2, c) gel 1 + 0.025 wt% ox-CNTs, d) gel 2 + 0.025 wt% ox-CNTs, e) gel 1 + 0.025 wt% GO, and f) gel 2 + 0.025 wt% GO, at different time points.

Similarly, the CD spectrum of gel 2 showed no signal at t0 with the appearance of characteristic bands after 1 h of gelation (Figure 4b). Indeed, a negative band was also observed at ~220 nm, as well as another negative band between 270 and 310 nm, which looks like a sort of mirror image of the band obtained for gel 1 in this region.

We observed instead a difference in the hydrogelation kinetics for the hybrid CNT-based gels. For both gel 1 and gel 2 the hydrogelation was more rapid, showing CD signals already at t0 (Figure 4c-d). The presence of the ox-CNTs in the hydrogel matrix had no impact on the structural organization of the fibrils as similar bands appeared in both cases. For the gels containing GO we also observed similar bands and kinetics in comparison with the native gels

(Figure 4e-f). As control we analyzed an aqueous suspension of ox-CNTs or GO at similar concentrations and no CD signals were observed (Figure S4), allowing to conclude that ox-CNTs and GO do not interfere with the CD measurements. Compared to the two-dimensional shape of the GO sheets, the quasi-one-dimensional tubular shape of the ox-CNTs, probably facilitates the interactions with the gel fibrils, which accelerates the gelation process.

2.5. Rheological study

Both hydrogels were characterized by rheology (oscillatory time and frequency sweep) to assess the time of gelation and their viscoelastic properties. Time sweeps were first performed by monitoring the evolution of the real part G' and imaginary part G" of the complex shear modulus as a function of time for native gel 1 (Figure 5a) and gel 2 (Figure 5b). A gradual change in behavior from a liquid (G'<G") to a solid state (G'> G") was observed for both gels ~10 min after adding water to the solution of the amino acids in DMSO (Figure S5). A second growth regime was noticed approximatively 5 h after the gelation, showing a much slower change in the hydrogel rheological response over time. This regime was associated with an aging phenomenon, which is also usually found in polymer gels[50,51] and organogels,[52,53] corresponding to the progressive strengthening of the elastic network. In this regime, the evolution of the complex shear modulus with frequency (Figure 5, insets) revealed a behavior, which is similar to many organogels[53,54] and physical gels.[55,56] Indeed, a low frequency behavior characterized by a plateau was observed for G' and G". Both gel 1 and gel 2 displayed similar G' values, indicating that these two systems have almost the same modulus of rigidity. Regarding the G" values, the hydrodynamic regime was reached in a slightly lower frequency range for gel 1 compared to gel 2. This small difference could be due to the presence of larger heterogeneities in size and number for gel 1 compared to gel 2, which was confirmed by the photographs of the hybrid gels in Figure 2. These heterogeneities could also explain the slight successive slope failures observed for gel 1 in the first part of the gel formation kinetics curve.

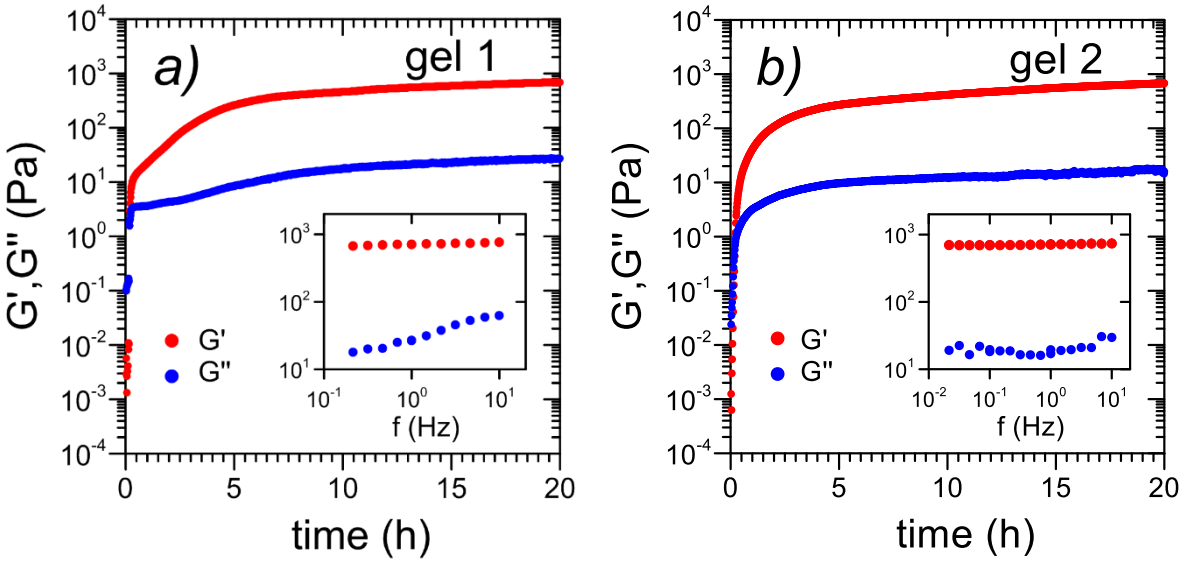

Figure 5. Evolution of the real part G' and imaginary part G" of the shear modulus for a) gel 1 and b) gel 2. The frequency was 1 Hz and the temperature was 20°C. The inset figures correspond to the variation of G' and G" as a function of frequency, measured 20 h after the gel formation.

The rheological studies were then extended to the hybrid gels. As the native gel 1 and gel 2 displayed similar rheological behavior, we have decided to show hereafter only the results of gel 1 containing GO or ox-CNTs at a concentration of 0.025 wt %. The incorporation of the carbon nanomaterials in gel 1 did not change its rigidity, which remained quite similar to that of the native gel (Figure 6). Likewise, the response in frequency of both hybrid gels was not affected by the presence of GO or ox-CNTs, suggesting that the structure of the fibrillar network was not altered by the presence of GO and ox-CNTs, as we also showed by TEM (Figure 3e-h). Generally, carbon nanomaterials are used as reinforcing agents into hydrogels due to the mechanical strength of CNTs and graphene-based nanomaterials (using higher concentrations in comparison to our study). These characteristics can be exploited for tissue engineering.[28,57] But, in our case similar rheological properties were expected between the native gels and hybrid gels due to the very low concentration of carbon nanomaterials, which is however sufficient to induce a photothermal effect (*vide infra*). Nevertheless, the kinetics of gelation was affected and was found to be strongly dependent on the shape of the carbon nanomaterials. Indeed, the gelation time was slightly reduced for GO-loaded gel 1, whereas it was so low when ox-CNTs were incorporated into the gel, that it could not be measured during our experiments (Figure S6a-b). In the latter case the faster gelation time could be explained by the tubular shape of the CNTs, which favors tight interactions with the amino acid fibrils compared to the two-

dimensional shape of the GO sheets, as previously observed by TEM (Figure 3e-h). These results are also in good agreement with CD showing a faster gelation time for CNT-loaded gels (Figure 4c-d). The altered gelation time, which is linked to the shape of the carbon nanomaterials, suggests that the gelation mechanism is driven by a nucleation growth process, in which the CNTs promote the nucleation of the fibrils. To support this hypothesis, shear measurements were performed on gel 1 loaded with ox-CNTs at a concentration 10 times lower (0.0025 wt%). The gelation time found for this concentration was ~4 min (Figure S6c), a value intermediate between the time for the gel at the concentration of 0.025 wt% (< 1 min) and that of the native gel (10 min). This result shows that the gelation time can be fully monitored by the amount of ox-CNTs loaded in the gel.

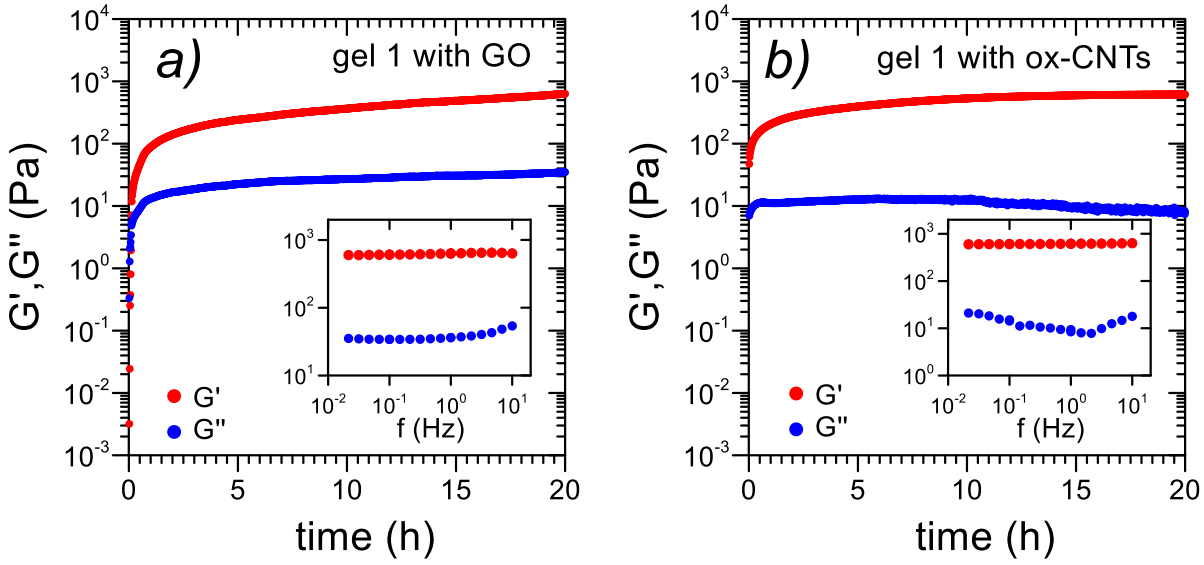

Figure 6. Evolution of G' and G" for gel 1 loaded with a) GO and b) ox-CNTs. The frequency was 1 Hz and the temperature was 20°C. The inset figures correspond to the variation of G' and G" as a function of frequency, measured 20 h after the gel formation.

2.6. Computational analysis

To highlight the main interactions that lead to the hydrogel formation, we decided to perform MD simulations. Both gel 1 and gel 2 were simulated at different concentrations of protected amino acids either in 2% DMSO/H_2O (v/v) solution or in pure DMSO (see Table S2 for the composition of the simulated systems). Each solution was simulated for at least 50 ns. Final snapshots are given in Figure 7 and Figure S7. Both mixtures show the same behavior in aqueous solution with the formation of aggregates during the dynamics, independently of the initial concentration. The conclusions are quite different in pure DMSO where the protected amino acids stay well-dispersed in the box. These results can explain why the gelation process

needs a two-step procedure with a first dilution in DMSO, allowing to solubilize the amino acids, followed by the dilution in water where the nano-arrangement occurs. More specifically, as illustrated in Figure 7, the aggregation of the protected amino acids is induced in DMSO/H_2O by specific π–π and CH–π interactions. Table S3 gives the average number of these interactions among the dynamics. For all the simulated systems, the principal π–π interactions are between the aromatic group of tyrosine and the Fmoc protecting group (Figure 7), followed by all the interactions where the Fmoc group is involved (Fmoc/Fmoc, Fmoc/Bzl and Fmoc/Phe) and the Tyr/Tyr interactions. These simulations support the results observed by CD. At low (10+10) and high (60+60) concentration of amino acids, the number of π–π interactions is quite similar in the two gels (7.4 *vs* 6.0 at 10+10 and 36.7 *vs* 38.7 at 60+60). At medium concentration, the Fmoc-Tyr-OH/Fmoc-Tyr(Bzl)-OH mixture forms twice as much interactions than Fmoc-Phe-OH/Fmoc-Tyr(Bzl)-OH (13.1 *vs* 26.1). This difference is due to a larger amount of interactions between the Fmoc and Tyr moieties leading to a more compact aggregate. Jointly to these aromatic attractions, the molecules also interact *via* H-bonds between the amino acid groups. The amount of H-bonds as a function of the concentration follows the same order than the aromatic interactions with similar number of H-bonds at low (10+10) and high (60+60) concentration of amino acids (2.0 *vs* 3.2 at 10+10 and 15.3 *vs* 10.8 at 60+60). At medium concentration (30+30) Fmoc-Tyr-OH/Fmoc-Tyr(Bzl)-OH mixture also forms twice as much H-bonds than Fmoc-Phe-OH/Fmoc-Tyr(Bzl)-OH does (3.7 *vs* 6.3). These additional aromatic interactions and hydrogen bonding induced by the presence of the hydroxyl group of tyrosine may explain the difference in fibril diameters between both systems observed by microscopy.

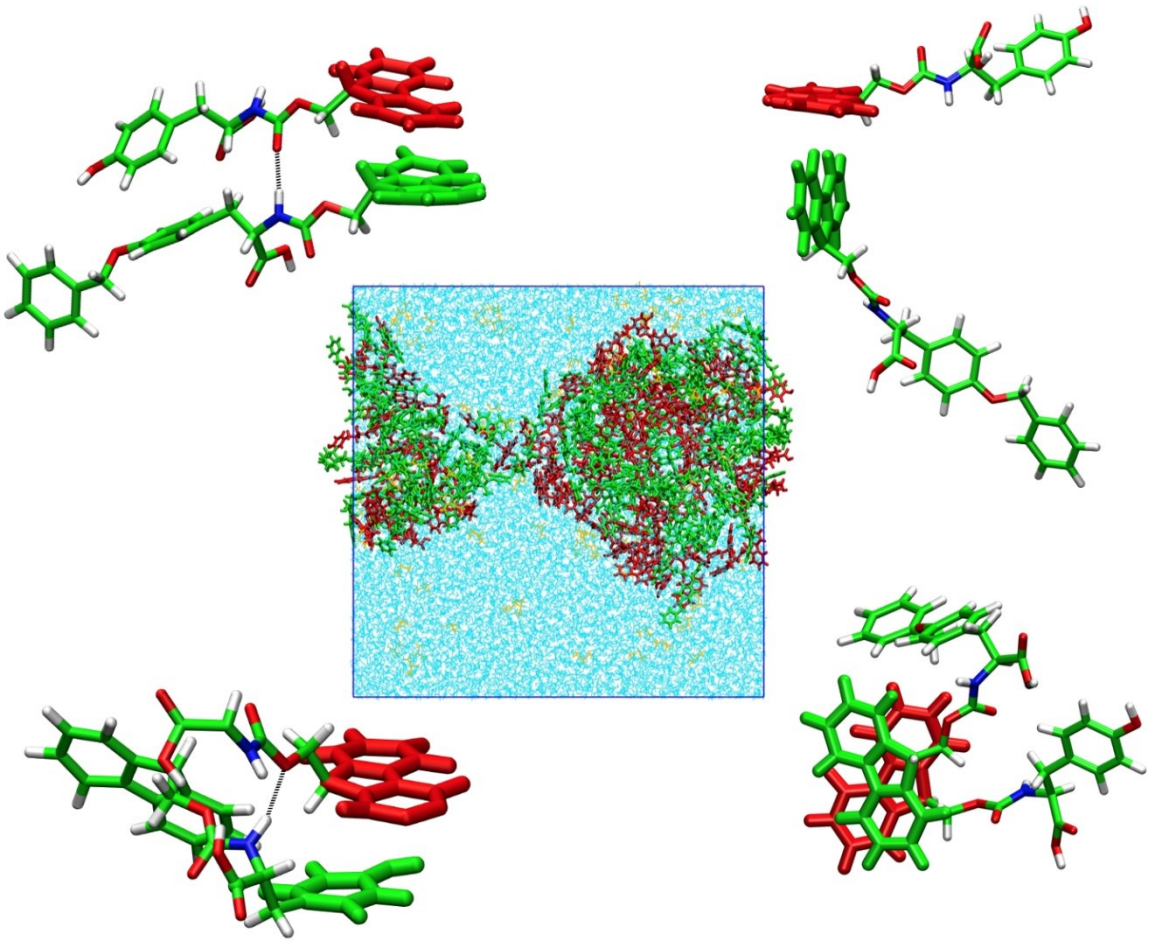

Figure 7. Final snapshots of the 60 Fmoc-Tyr-OH + 60 Fmoc-Tyr(Bzl)-OH system simulated in 2% DMSO/H_2O (v/v) showing typical π-π and CH-π arrangements between the two components. In the box Fmoc-Tyr-OH molecules are represented in red and Fmoc-Tyr(Bzl)-OH in green.

2.7. Photothermal study

After thoroughly analyzing the structure and the mechanical properties of the native and hybrid gels, we investigated their photothermal properties. For this purpose, the photothermal conversion of different concentrations of suspensions of ox-CNTs and GO alone in water was first examined by monitoring the temperature increase during exposure to NIR light irradiation (at 808 nm, under 2 W for 10 min). At each concentration a similar dose-dependent photothermal behavior was observed for both ox-CNTs and GO (Figure S8). The temperature increase was 20°C, 28°C, and 47°C in 10 min for a concentration of 0.005 wt%, 0.01 wt%, and 0.025 wt%, respectively. The native and hybrid gels were also studied in similar conditions. The change in temperature for both gel 1 and gel 2 was very low with an increase of less than 5°C after 10 min of irradiation as expected and the gels remained totally intact (Figure 8).

Hybrid gel 1 showed a similar temperature increase whatever it contained ox-CNTs or GO, which was not the case for gel 2. Indeed, after 10 min of irradiation the temperature difference was 40-41°C for gel 1 + ox-CNTs or GO, and gel 2 + GO, whereas the temperature increase was 47°C for gel 2 + ox-CNTs. The presence of ox-CNTs, which accelerates the hydrogelation process for both gels, also improves the increase of temperature during NIR irradiation in the case of gel 2. In addition, the gel structure slightly reduces the heating capacity of the carbon nanomaterials compared to their suspensions in water except for gel 2 + ox-CNTs reaching 47°C. Interestingly, we observed that in presence of ox-CNTs or GO the hybrid gel 1 was destructured, while the hybrid gel 2 shrank and formed a compact block (Figure S9). This result is concordant with a more homogeneous three-dimensional fibrous network in gel 2. It seems that the presence of the hydroxyl group of tyrosine not only influences the fibril diameter, but it can also decrease the structural stability of the gel in presence of the carbon nanomaterials.

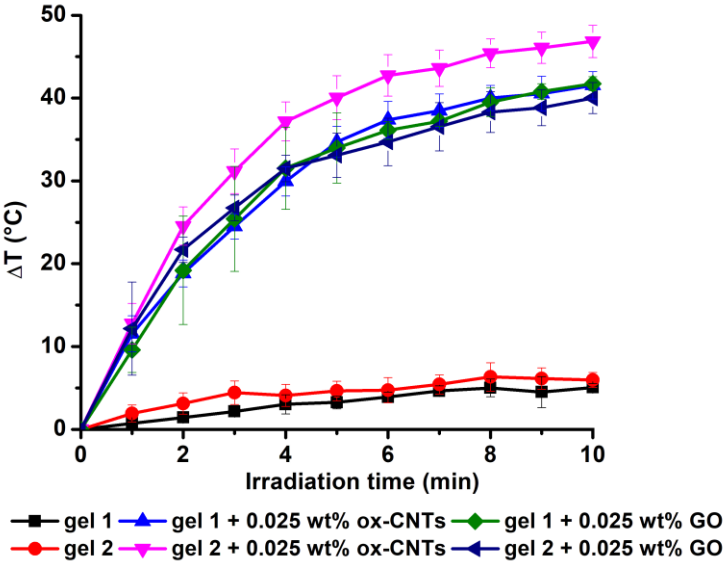

Figure 8. Temperature increase of the native gels in comparison to the hybrid gels when exposed to a NIR laser (at 808 nm, under 2 W) as a function of the laser irradiation time.

2.8. Photothermal drug release

To prove that our hydrogels have potential therapeutic applications, we decided to study the release of a model drug encapsulated into the gels, triggered by irradiation in the NIR region. Commonly known as vitamin C, L-ascorbic acid has a wide range of clinical applications and it was selected as hydrophilic drug model. It promotes collagen biosynthesis, has antiscorbutic properties and protects against photoaging, UV-induced immunosuppression, and photocarcinogenesis.[58,59] To prepare the drug-loaded hydrogels, L-ascorbic acid was first dissolved in water before the addition of the solution of Fmoc-Tyr-OH/Fmoc-Tyr(Bzl)-OH

(leading to gel 1) or Fmoc-Phe-OH/Fmoc-Tyr(Bzl)-OH (leading to gel 2) in DMSO. The gelation was monitored using the vial inversion test. After approximately 2 h both L-ascorbic acid-loaded gel 1 and gel 2 formed a stable hydrogel. We observed a higher stability of L-ascorbic acid loaded in the gels over time (Figure S10). A range of drug concentration (0.2-1.5 $mg \cdot mL^{-1}$) was studied and we observed that a concentration of 0.7 $mg \cdot mL^{-1}$ (4 mM) of L-ascorbic acid was the maximum concentration that can be incorporated into the hydrogels. Above this concentration the gelation process was disturbed with the appearance of a liquid phase. The mass concentration is in the range of drug loadings such as insulin and doxorubicin reported for some hydrogels containing carbon nanomaterials (0.08 to 2 $mg \cdot mL^{-1}$).[60-62] But, if we consider molar concentration, our loading value is higher compared to these studies (4 mM *vs.* 14 µM to 3.7 mM of drug). To prepare the drug-loaded hybrid gels, the ox-CNTs or GO were dispersed at a concentration of 0.025 wt% into a 0.7 $mg \cdot mL^{-1}$ solution of L-ascorbic acid before addition to the solution of the amino acids in DMSO. The drug release was investigated by irradiating the four hybrid gels containing L-ascorbic acid. The temperature of the hydrogels was monitored during the irradiation (Figure S11). Control experiments were performed on the gels devoid of carbon nanomaterials containing L-ascorbic acid. The volume of water released from the gels was measured after 10 min irradiation and the concentration of the released drug was determined by HPLC. We verified that L-ascorbic acid remains stable in these conditions. As expected, the control gels did not show any release of water and drug after 10 min irradiation (data not shown). On the contrary, in the presence of ox-CNTs or GO, gel 1 released 68% and 73% of water, respectively, whereas gel 2 released a higher amount of water (84% and 79%, respectively) (Figure 9a). As previously observed, the hybrid gel 1 loaded with L-ascorbic acid showed a structural destruction of the gel matrix upon NIR light irradiation whatever it contains ox-CNTs or GO, while the hybrid gel 2 shrank leading to the formation of a compact block. Therefore, the lower volume of water released from the hybrid gel 1 containing ox-CNTs or GO is probably due to the destabilization of the gel structure during the irradiation. The higher water release capacity of gel 2 + ox-CNTs reveals a better photothermal behavior compared to the other hybrid gels, as observed in Figure 8. This remarkable feature is probably linked to the higher homogeneity of the three-dimensional fibrous network in gel 2, as previously mentioned. The drug concentration was assessed by HPLC and the four hybrid gels showed a drug release comprised between 63% and 82% after 10 min irradiation (Figure 9b). The gel 2 + ox-CNTs was found to be the most efficient system with a maximum drug release of 82%. The amount of L-ascorbic acid release can be correlated to the water release capacity of the hydrogels. Overall, these results show that the drug release is triggered by the heat generation from the ox-

CNTs or GO upon NIR light irradiation. We have investigated the drug release over time for the 4 different gels and observed that a plateau was reached after 8 to 10 min (Figure S12). The amount of drug released from the gels is primarily influenced by the nature of the amino acids constituting the hydrogel and the type of carbon nanomaterials has also some influence. We found that gel 2 loaded with the ox-CNTs was the most efficient gel and this was correlated with the highest water release and best photothermal capacity observed for ox-CNT-loaded gel 2. This was probably due to a higher homogeneity of the 3D fibrous network in gel 2 and well-distributed ox-CNTs in the gel. The high liberation of L-ascorbic acid reached in our study is similar or higher than NIR irradiation-induced drug release rates reported for other types of carbon nanomaterial-containing hydrogels.[60,61,63] In addition, we performed preliminary stability experiments in physiological saline solution (0.9% NaCl) and in RPMI or DMEM supplemented with 10% fetal bovine serum. For this purpose, a volume of 100 µL of physiological saline solution or 10% fetal bovine serum in culture medium was added on top of each hydrogel (400 µL). After 15 h the solution was withdrawn and the amount of L-ascorbic acid was determined by HPLC. We observed that the hydrogels were not degraded when exposed to physiological saline solution (0.9% NaCl). We noticed that a small amount of water was released only from the hybrid gels 2 (Figure S13a). We estimated that 15 to 21% of L-ascorbic acid was liberated from the four hydrogels by diffusion. In 10% fetal bovine serum in culture medium we found that the hybrid gels 1 were less stable and released a significant volume of water, which was not the case for the hybrid gels 2 (Figure S13b-c). This result was correlated with a higher amount of L-ascorbic acid released from the hybrid gels 1 (12-51%), whereas only 8 to 12% of drug were liberated from the hybrid gels 2. These stability experiments show that the hybrid gels 2 are more stable in physiological conditions and this is probably related to the higher homogeneity of the 3D fibrous network in gel 2. These results support the fact that gel 2 is more efficient compared to gel 1 for our purpose of controlled drug release. Overall, our hydrogels present many advantages such as i) simple preparation as they are constituted of commercial amino acids, ii) low content of carbon nanomaterials, iii) high drug loading and release capacity, and iv) stability in physiological conditions (in particular for gel 2).

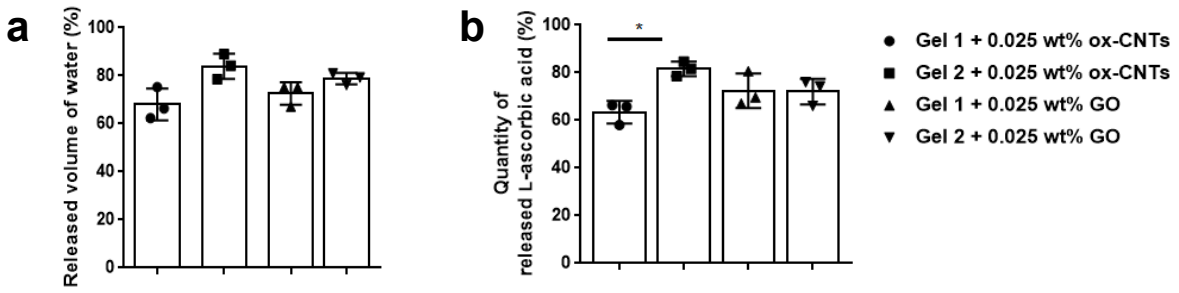

Figure 9. Release of a) water (n=3) and b) L-ascorbic acid (n=3) from the hybrid gels under NIR light irradiation. Statistical analysis was performed by one-way ANOVA (including Bonferroni's multiple comparison test).

3. Conclusions

We have demonstrated the spontaneous self-assembly of different commercially available Fmoc-protected amino acids into three-dimensional fibrous network leading to the formation of hydrogels. We have investigated more in detail the gelation of a binary mixture composed of Fmoc-Tyr-OH/Fmoc-Tyr(Bzl)-OH or Fmoc-Phe-OH/Fmoc-Tyr(Bzl)-OH. The structural and physical properties of these gels were assessed using various microscopic techniques and rheology. The hydrogel formation was mainly driven by aromatic interactions, as supported by CD and MD simulations. Oxidized CNTs and GO were incorporated in these hydrogels and they showed good interfacing with the fibrils, in particular the nanotubes. L-Ascorbic acid was loaded in the gels as model hydrophilic drug at a high concentration. The heat generated by the carbon nanomaterials upon NIR light irradiation induced the release of the drug at a high rate. These novel self-assembled hydrogels open up the possibilities of various applications and they will be explored further for drug delivery. As future work we plan to perform experiments using different types of cells to validate our approach of controlled drug delivery *in vitro*. We will also extend the study to other types of drugs, in particular hydrophobic drugs.

4. Experimental section

4.1. Materials and methods

The amino acids L-tyrosine, L-histidine, L-tryptophan, Fmoc-Tyr(*t*Bu)-OH, H-Tyr(Bzl)-OBzl·HCl, Z-Tyr-OMe, and Fmoc-Trp-OH were purchased from Sigma-Aldrich, and L-phenylalanine from Neo-MPS, respectively. H-Tyr-OBzl, Fmoc-Tyr(Bzl)-OH, and Z-Tyr(Bzl)-OH were acquired from Bachem, and Fmoc-Phe-OH, Fmoc-Tyr-OH, and Fmoc-His-OH from PolyPeptide Group. RPMI-1640 Medium and Dulbecco's Modified Eagle

Medium were purchased from Sigma-Aldrich and Lonza, respectively, and fetal bovine serum from Dominique Dutscher. The pristine multi-walled CNTs (20-30 nm diameter, 0.5-2 μm length, 95% purity; batch 1240XH) were purchased from Nanostructured and Amorphous Materials. The CNTs were oxidized following the protocol we reported in a previous work.[64] GO was obtained from Grupo Antolin. All other reagents were obtained from different commercial suppliers and used as received. The ultrasonic treatments were performed in an ultrasonic bath Elmasonic P (100 W, 37 kHz). A 808 nm laser diode system from Roithner Lasertechnik (LOS-BLD-0808-2W-C/P) and a thermal imaging camera from Flir One were used for the photothermal studies. The centrifugation was done with a centrifuge 5415 R from Eppendorf. HPLC was performed using a Nucleosil 100-5 Waters C_{18} reverse phase HPLC column and a Waters Alliance e2695 separation module. The column was used with 1.2 $mL \cdot min^{-1}$ flow rate of a gradient from 0 to 100% of B (A = H_2O/0.1% TFA; B = CH_3CN/0.08% TFA) for 20 min.

4.2. Gel preparation

Each monomer was dissolved in DMSO to make stock solutions of 247 mM. Single amino acid systems were prepared by dilution of the monomers from the stock solutions in MilliQ® water to reach a concentration of 4.9 mM in 2% DMSO/H_2O (v/v). Binary mixtures were prepared by mixing each monomer from the stock solutions in a 1:1 ratio followed by dilution in MilliQ® water to a final concentration of 4.9 mM (2.45 mM of each monomer) in 2% DMSO/H_2O (v/v). After dilution each sample was sonicated in a water bath for 10 sec and left under ambient conditions. The gelation of the samples was confirmed by the vial inversion test by turning the vials upside down and observe whether the hydrogel is stable or not.

4.3. Incorporation of pristine CNTs, oxidized CNTs, and GO

The pristine CNTs, ox-CNTs, or GO were dispersed in MilliQ® water at three different concentrations: 255 $\mu g \cdot mL^{-1}$ (0.025 wt%), 1.26 $mg \cdot mL^{-1}$ (0.1 wt%), and 6.3 $mg \cdot mL^{-1}$ (0.5 wt%). The suspensions were added to the amino acid solution of gel 1 or gel 2 in DMSO (247 mM) to reach a final concentration of monomer of 4.9 mM in 2% DMSO/H_2O (v/v). The suspensions were sonicated for 10 s in a water bath and left under ambient conditions.

4.4. Scanning electron microscopy

SEM analysis was performed on a SEM S-800 (Hitachi High Technologies Corporation, Tokyo, Japan) with an accelerative voltage of 5 kV. The samples were placed onto glass slides and then

allowed to stand for 1 h, after which the sample was removed by capillary action (filter paper). The samples were metallized by sputtering with Au/Pt (SCD030 BALZERS).

4.5. Transmission electron microscopy

TEM analysis was performed with a Hitachi 7500 transmission electron microscope (Hitachi High Technologies Corporation, Tokyo, Japan) with an accelerative voltage of 80 kV equipped with an AMT Hamamatsu digital camera (Hamamatsu Photonics, Hamamatsu City, Japan). To prepare the TEM samples, 10 µL of each hydrogel was deposited onto a carbon-coated copper grid (Formvar/Carbon 300 Mesh; Cu from Delta Microscopies). The gel was allowed to stand for 1-2 min, after which the sample was removed by capillarity using a filter paper. The grid was allowed to dry under ambient condition.

4.6. Circular dichroism

The binary mixture of amino acids in 2% DMSO/H_2O (v/v) were prepared and after sonication the solutions were directly transferred into a 0.05 mm path length quartz cuvette. CD spectra were recorded on a JASCO J-810 spectropolarimeter. Spectra were collected at room temperature from 350-190 nm with 1.0 nm step, a scanning speed of 100 $nm \cdot min^{-1}$, and 1 s integration time.

4.7. Rheological study

Rheological properties were investigated using a controlled-stress rheometer (Haake, Mars III) working in oscillatory mode. The measuring cell used was concentric cylinders (Couette cell type). For the rheological study, the same protocol was followed for the sample preparation and for the shear measurements. Once prepared, the sample still in its liquid state, was introduced in the Couette cell and measurements of the complex shear modulus were performed over time to follow the evolution of the shear response from the liquid state to the gel state. The frequency *f* and the stress to the sample applied σ were 1 Hz and 0.2 Pa, respectively. After 20 h, these measurements were followed by shear measurements performed as a function of frequency. All the measurements were carried out at room temperature (20°C).

4.8. Computational analysis

4.8.1. Computational methods

The binary mixtures have been simulated by classical MD simulations using the AMBER16 software,[65] in which the potential energy U is empirically represented by a sum of bond, angle

and dihedral deformations and by pair wise additive 1-6-12 (electrostatic + van der Waals) interactions between non-bonded atoms:

$$U = \sum_{bonds} k_b(r - r_0)^2 + \sum_{angles} k_\theta(\theta - \theta_0)^2 + \sum_{dihedrals} V_n[1 + cos(n\phi - \gamma)] + \sum_{i=1}^{N-1} \sum_{j=i+1}^{N} \left[\frac{A_{ij}}{R_{ij}^{12}} - \frac{B_{ij}}{R_{ij}^{6}} + \frac{q_i q_j}{\varepsilon_0 r_{i,j}}\right]$$

Cross terms in van der Waals interactions were constructed using the Lorentz-Berthelot rules. Water was represented with the TIP3P model[66] and DMSO by the model developed by Fox and Kollman.[67] Fmoc molecules were represented with the parameters from AMBER99 force field and RESP charges. The 1-4 van der Waals and 1-4 coulombic interactions were scaled down by 2.0 and 1.2, respectively. The solutions were simulated with 3D-periodic boundary conditions, using an atom-based cutoff of 12 Å for non-bonded interactions, and correcting for the long-range electrostatics by using the Ewald summation method. The characteristics of all simulated systems are given in Table S2. The MD simulations were performed at 300 K starting with random velocities. The temperature was monitored *via* a coupling to a thermal bath using the Berendsen algorithm[68] with a relaxation time of 0.2 ps. In the (NPT) simulations, the pressure was similarly coupled to a barostat with a relaxation time of 0.2 ps. A time step of 2 fs was used to integrate the equations of motion *via* the Verlet leapfrog algorithm. For each system, a "random" mixture of the two amino acids was prepared in a box of water:DMSO 98:2 (see Table S2 for exact composition of each systems). After 1000 steps of energy minimization, 0.25 ns of dynamics were performed with ions in order to allow the solvent to relax around the solute. This was followed by a dynamics of 0.25 ns at constant volume and of 1 ns at a constant pressure of 1 atm. The evolution of the mixture was then followed for 50 to 300 ns of dynamics (NVT ensemble).

4.8.2. Analysis of the results

The trajectories were analyzed using our MD simulations software.[69] Snapshots were drawn with the VMD software.[70]

4.9. Photothermal study

Different concentrations of ox-CNTs and GO in MilliQ® water (0.005 wt%, 0.01 wt%, and 0.025 wt%) were sonicated for 10 min to obtain highly dispersed suspensions. Native and hybrid gels were synthesized and left for gelation for 2 h under ambient conditions. The photothermal conversion of the carbon nanomaterial suspensions and the heating profile of

the gels were examined by monitoring the temperature increase during exposure to 808 nm laser with a power of 2 W for 10 min and a laser-sample distance of 3 cm. Each photothermal measurement was repeated three times. Maximum temperatures and infrared thermographic maps were recorded by an infrared thermal imaging camera.

4.10. Release of L-ascorbic acid

To prepare the L-ascorbic acid-loaded hydrogels, the amino acid solutions of Fmoc-Tyr-OH/Fmoc-Tyr(Bzl)-OH (gel 1) or Fmoc-Phe-OH/Fmoc-Tyr(Bzl)-OH (gel 2) in DMSO were diluted in a solution of L-ascorbic acid in MilliQ® water (0.7 $mg \cdot mL^{-1}$). The hybrid gels were obtained by dispersing the ox-CNTs or GO at a concentration of 255 $\mu g \cdot mL^{-1}$ (0.025 wt%) in a solution of L-ascorbic acid in MilliQ® water (0.7 $mg \cdot mL^{-1}$). After sonication for 10 min in a water bath, the amino acid solution in DMSO was added. The suspensions were sonicated for 10 s in a water bath and left under ambient conditions. NIR light irradiation (at 808 nm, under 2 W for 10 min, at a distance of 3 cm from the gels) was applied on the gels after 2 h of gelation to avoid any significant drug degradation. The volume of released water was withdrawn, centrifuged (12300 rpm, 10 min), and the amount of L-ascorbic acid was assessed by HPLC (t_r = 2.3 min at λ = 254 nm for L-ascorbic acid). Statistical analysis was performed with Prism 7.0 (GraphPad Software). Data were analyzed with one-way-ANOVA (including Bonferroni multiple comparison test). A p value of < 0.05 was considered as significant.

4.11. Preliminary stability studies in physiological conditions

A volume of 100 µL of physiological saline solution (0.9% NaCl in MilliQ® water) or RPMI or DMEM supplemented with 10% fetal bovine serum was added on top of each hydrogel (400 µL). After 15 h the solution was withdrawn, centrifugated (12300 rpm, 5 min) , and the amount of L-ascorbic acid was determined by HPLC.

Associated content

Supporting Information

Structures of the aromatic amino acids derivatives; table summarizing all the gelation tests performed using a variety of amino acid derivatives; photographs of the hybrid gels; diameter distribution of the amino acid fibrils; evolution of G' and G" *vs.* time for gel 1 and gel 2; table describing the simulated systems; snapshots of the simulated mixed systems; table summarizing the π-π interactions and H-bonds in the simulated systems; kinetics of the temperature increase

for aqueous suspensions of ox-CNT or GO suspensions and for the hybrid gels loaded with L-ascorbic acid upon NIR irradiation; photographs of the hybrid gels after NIR irradiation.

Author information

Corresponding Authors

*E-mail: c.menard@ibmc-cnrs.unistra.fr , a.bianco@ibmc-cnrs.unistra.fr

Acknowledgements

This work was supported by the Centre National de la Recherche Scientifique (CNRS), by the Agence Nationale de la Recherche (ANR) through the LabEx project Chemistry of Complex Systems (ANR-10-LABX-0026_CSC), and by the International Center for Frontier Research in Chemistry (icFRC). The authors wish to acknowledge Cathy Royer and Valérie Demais for TEM and SEM analyses at the "Plateforme Imagerie in Vitro" at the Center of Neurochemistry (Strasbourg, France).

References

(1) Bentley, W. E.; Payne, G. F. Materials Science. Nature's Other Self-Assemblers. *Science* **2013**, *341*, 136–137.

(2) Oliva, N.; Conde, J.; Wang, K.; Artzi, N. Designing Hydrogels for On-Demand Therapy. *Acc. Chem. Res.* **2017**, *50*, 669–679.

(3) Motealleh, A.; Kehr, N. S. Nanocompoite Hydrogels and Their Applications in Tissue Engineering. *Adv. Healthc. Mater.* **2017**, *6*, 1600938.

(4) Ryan, D. M.; Nilsson, B. L. Self-Assembled Amino Acids and Dipeptides as Noncovalent Hydrogels for Tissue Engineering. *Polym. Chem.* **2011**, *3*, 18–33.

(5) Tao, K.; Makam, P.; Aizen, R.; Gazit, E. Self-Assembling Peptide Semiconductors. *Science* **2017**, *358*, eaam9756.

(6) Vigier-Carrière, C.; Boulmedais, F.; Schaaf, P.; Jierry, L. Surface-Assisted Self-Assembly Strategies Leading to Supramolecular Hydrogels. *Angew. Chem. Int. Ed. Engl.* **2018**, *57*, 1448–1456.

(7) Tian, R.; Chen, J.; Niu, R. The Development of Low-Molecular Weight Hydrogels for Applications in Cancer Therapy. *Nanoscale* **2014**, *6*, 3474–3482.

(8) Raeburn, J.; Zamith Cardoso, A.; Adams, D. J. The Importance of the Self-Assembly Process to Control Mechanical Properties of Low Molecular Weight Hydrogels. *Chem. Soc. Rev.* **2013**, *42*, 5143–5156.

(9) Tao, N.; Li, G.; Liu, M.; Gao, W.; Wu, H. Preparation of Dual Responsive Low-Molecular-Weight Hydrogel for Long-Lasting Drug Delivery. *Tetrahedron* **2017**, *73*, 3173–3180.

(10) Rajbhandary, A.; Raymond, D. M.; Nilsson, B. L. Self-Assembly, Hydrogelation, and Nanotube Formation by Cation-Modified Phenylalanine Derivatives. *Langmuir* **2017**, *33*, 5803–5813.

(11) Dasgupta, A.; Mondal, J. H.; Das, D. Peptide Hydrogels. *RSC Adv.* **2013**, *3*, 9117–9149.

(12) Iglesias, D.; Melle-Franco, M.; Kurbasic, M.; Melchionna, M.; Abrami, M.; Grassi, M.; Prato, M.; Marchesan, S. Oxidized Nanocarbons-Tripeptide Supramolecular Hydrogels: Shape Matters! *ACS Nano* **2018**, *12*, 5530–5538.

(13) Aggeli, A.; Boden, N.; Carrick, L. M.; Mcleish, T. C. B.; Nyrkova, I. A.; Semenov, A. N. Self-Assembling Peptide Gels. In *Molecular Gels: Materials with Self-Assembled Fibrillar Networks*; Weiss, R. G., Terech, P., Eds.; Springer Netherlands: Dordrecht, 2006; pp 99–130.

(14) Sutton, S.; Campbell, N. L.; Cooper, A. I.; Kirkland, M.; Frith, W. J.; Adams, D. J. Controlled Release from Modified Amino Acid Hydrogels Governed by Molecular Size or Network Dynamics. *Langmuir* **2009**, *25*, 10285–10291.

(15) Eskandari, S.; Guerin, T.; Toth, I.; Stephenson, R. J. Recent Advances in Self-Assembled Peptides: Implications for Targeted Drug Delivery and Vaccine Engineering. *Adv. Drug Deliv. Rev.* **2017**, *110–111*, 169–187.

(16) Kumar, D.; Workman, V. L.; O'Brien, M.; McLaren, J.; White, L.; Ragunath, K.; Rose, F.; Saiani, A.; Gough, J. E. Peptide Hydrogels-A Tissue Engineering Strategy for the Prevention of Oesophageal Strictures. *Adv. Funct. Mater.* **2017**, *27*, 1702424.

(17) Koutsopoulos, S. Self-Assembling Peptide Nanofiber Hydrogels in Tissue Engineering and Regenerative Medicine: Progress, Design Guidelines, and Applications. *J. Biomed. Mater. Res. A* **2016**, *104*, 1002–1016.

(18) Ma, M.; Kuang, Y.; Gao, Y.; Zhang, Y.; Gao, P.; Xu, B. Aromatic-Aromatic Interactions Induce the Self-Assembly of Pentapeptidic Derivatives in Water to Form Nanofibers and Supramolecular Hydrogels. *J. Am. Chem. Soc.* **2010**, *132*, 2719–2728.

(19) Nanda, J.; Biswas, A.; Banerjee, A. Single Amino Acid Based Thixotropic Hydrogel Formation and pH-Dependent Morphological Change of Gel Nanofibers. *Soft Matter* **2013**, *9*, 4198–4208.

(20) Draper, E. R.; Morris, K. L.; Little, M. A.; Raeburn, J.; Colquhoun, C.; Cross, E. R.; McDonald, T. O.; Serpell, L. C.; Adams, D. J. Hydrogels Formed from Fmoc Amino Acids. *CrystEngComm* **2015**, *17*, 8047–8057.

(21) Orbach, R.; Mironi-Harpaz, I.; Adler-Abramovich, L.; Mossou, E.; Mitchell, E. P.; Forsyth, V. T.; Gazit, E.; Seliktar, D. The Rheological and Structural Properties of Fmoc-Peptide-based Hydrogels: The Effect of Aromatic Molecular Architecture on Self-assembly and Physical Characteristics. *Langmuir* **2012**, *28*, 2015–2022.

(22) Bhattacharya, S.; Samanta, S. K. Soft-Nanocomposites of Nanoparticles and Nanocarbons with Supramolecular and Polymer Gels and Their Applications. *Chem. Rev.* **2016**, *116*, 11967–12028.

(23) Servant, A.; Bussy, C.; Al-Jamal, K.; Kostarelos, K. Design, Engineering and Structural Integrity of Electro-responsive Carbon Nanotube-based Hydrogels for Pulsatile Drug Release. *J. Mater. Chem. B* **2013**, *1*, 4593–4600.

(24) Adhikari, B.; Banerjee, A. Short Peptide Based Hydrogels: Incorporation of Graphene into the Hydrogel. *Soft Matter* **2011**, *7*, 9259–9266.

(25) Mba, M.; Jiménez, A. I.; Moretto, A. Templating the Self-Assembly of Pristine Carbon Nanostructures in Water. *Chem. Eur. J.* **2014**, *20*, 3888–3893.

(26) Roy, S.; Banerjee, A. Functionalized Single Walled Carbon Nanotube Containing Amino Acid Based Hydrogel: a Hybrid Nanomaterial. *RSC Adv.* **2012**, *2*, 2105–2111.

(27) Wang, H.; Chen, Q.; Zhou, S. Carbon-based Hybrid Nanogels: A Synergistic Nanoplatform for Combined Biosensing, Bioimaging, and Responsive Drug Delivery. *Chem. Soc. Rev.* **2018**, *47*, 4198–4232.

(28) Vashist, A.; Kaushik, A.; Vashist, A.; Sagar, V.; Ghosal, A.; Gupta, Y. K.; Ahmad, S.; Nair, M. Advances in Carbon Nanotubes-hydrogel Hybrids in Nanomedicine for Therapeutics. *Adv. Healthc. Mater.* **2018**, *7*, e1701213.

(29) Ha, W.; Zhao, X.-B.; Jiang, K.; Kang, Y.; Chen, J.; Li, B.-J.; Shi, Y.-P. A Three-Dimensional Graphene Oxide Supramolecular Hydrogel for Infrared Light-responsive Cascade Release of Two Anticancer Drugs. *Chem. Commun.* **2016**, *52*, 14384–14387.

(30) Merino, S.; Martín, C.; Kostarelos, K.; Prato, M.; Vázquez, E. Nanocomposite Hydrogels: 3D Polymer-nanoparticle Synergies for On-demand Drug Delivery. *ACS Nano* **2015**, *9*, 4686–4697.

(31) Dong, X.; Wei, C.; Liang, J.; Liu, T.; Kong, D.; Lv, F. Thermosensitive Hydrogel Loaded with Chitosan-Carbon Nanotubes for Near Infrared Light Triggered Drug Delivery. *Coll. Surf. B* **2017**, *154*, 253–262.

(32) Kumar, S.; Rani, R.; Dilbaghi, N.; Tankeshwar, K.; Kim, K.-H. Carbon Nanotubes: a Novel Material for Multifaceted Applications in Human Healthcare. *Chem. Soc. Rev.* **2017**, *46*, 158–196.

(33) Reina, G.; González-Domínguez, J. M.; Criado, A.; Vázquez, E.; Bianco, A.; Prato, M. Promises, Facts and Challenges for Graphene in Biomedical Applications. *Chem. Soc. Rev.* **2017**, *46*, 4400–4416.

(34) Delogu, L. G.; Venturelli, E.; Manetti, R.; Pinna, G. A.; Carru, C.; Madeddu, R.; Murgia, L.; Sgarrella, F.; Dumortier, H.; Bianco, A. Ex Vivo Impact of Functionalized Carbon Nanotubes on Human Immune Cells. *Nanomedicine (Lond.)* **2012**, *7*, 231–243.

(35) Marangon, I.; Ménard-Moyon, C.; Kolosnjaj-Tabi, J.; Béoutis, M. L.; Lartigue, L.; Alloyeau, D.; Pach, E.; Ballesteros, B.; Autret, G.; Ninjbadgar, T.; Brougham, D. F.; Bianco, A.; Gazeau, F. Covalent Functionalization of Multi-walled Carbon Nanotubes with a Gadolinium Chelate for Efficient T_1-Weighted Magnetic Resonance Imaging. *Adv. Funct. Mater.* **2014**, *24*, 7173–7186.

(36) Jain, S.; Thakare, V. S.; Das, M.; Godugu, C.; Jain, A. K.; Mathur, R.; Chuttani, K.; Mishra, A. K. Toxicity of Multiwalled Carbon Nanotubes with End Defects Critically Depends on Their Functionalization Density. *Chem. Res. Toxicol.* **2011**, *24*, 2028–2039.

(37) Jasim, D. A.; Murphy, S.; Newman, L.; Mironov, A.; Prestat, E.; McCaffrey, J.; Ménard-Moyon, C.; Rodrigues, A. F.; Bianco, A.; Haigh, S.; Lennon, R.; Kostarelos, K. The Effects of Extensive Glomerular Filtration of Thin Graphene Oxide Sheets on Kidney Physiology. *ACS Nano* **2016**, *10*, 10753–10767.

(38) Ali-Boucetta, H.; Bitounis, D.; Raveendran-Nair, R.; Servant, A.; Van den Bossche, J.; Kostarelos, K. Purified Graphene Oxide Dispersions Lack In Vitro Cytotoxicity and In Vivo Pathogenicity. *Adv. Healthc. Mater.* **2013**, *2*, 433–441.

(39) Bhattacharya, K.; Mukherjee, S. P.; Gallud, A.; Burkert, S. C.; Bistarelli, S.; Bellucci, S.; Bottini, M.; Star, A.; Fadeel, B. Biological Interactions of Carbon-Based Nanomaterials: from Coronation to Degradation. *Nanomedicine* **2016**, *12*, 333–351.

(40) Russier, J.; Ménard-Moyon, C.; Venturelli, E.; Gravel, E.; Marcolongo, G.; Meneghetti, M.; Doris, E.; Bianco, A. Oxidative Biodegradation of Single- and Multi-walled Carbon Nanotubes. *Nanoscale* **2011**, *3*, 893–896.

(41) Kurapati, R.; Russier, J.; Squillaci, M. A.; Treossi, E.; Ménard-Moyon, C.; Del Rio-Castillo, A. E.; Vazquez, E.; Samorì, P.; Palermo, V.; Bianco, A. Dispersibility-Dependent Biodegradation of Graphene Oxide by Myeloperoxidase. *Small* **2015**, *11*, 3985–3994.

(42) Jiang, B.-P.; Zhou, B.; Lin, Z.; Liang, H.; Shen, X.-C. Recent Advances in Carbon Nanomaterials for Cancer Phototherapy. *Chem. Eur. J.* **2018**, DOI: 10.1002/chem.201804383.

(43) Ryan, D. M.; Doran, T. M.; Nilsson, B. L. Complementary π-π Interactions Induce Multicomponent Coassembly into Functional Fibrils. *Langmuir* **2011**, *27*, 11145–11156.

(44) Galvao, J.; Davis, B.; Tilley, M.; Normando, E.; Duchen, M.R.; Cordeiro, M.F. Unexpected Low-dose Toxicity of the Universal Solvent DMSO. *FASEB J.* **2014**, *28*, 1317–1330.

(45) Lee, H.; Park, J. B. Evaluation of the Effects of Dimethylsulphoxide on Morphology, Cellular Viability, mRNA, and Protein Expression of Stem Cells Culture in Growth Media. *Biomed. Rep.* **2017**, *7*, 291–296.

(46) Jayawarna, V.; Smith, A.; Gough, J. E.; Ulijn, R. V. Three-Dimensional Cell Culture of Chondrocytes on Modified Di-phenylalanine Scaffolds. *Biochem. Soc. Trans.* **2007**, *35*, 535–537.

(47) Mahler, A.; Reches, M.; Rechter, M.; Cohen, S.; Gazit, E. Rigid, Self-Assembled Hydrogel Composed of a Modified Aromatic Dipeptide. *Adv. Mater.* **2006**, *18*, 1365–1370.

(48) Ryan, D. M.; Anderson, S. B.; Nilsson, B. L. The Influence of Side-chain Halogenation on the Self-Assembly and Hydrogelation of Fmoc-phenylalanine Derivatives. *Soft Matter* **2010**, *6*, 3220–3231.

(49) Smith, A. M.; Williams, R. J.; Tang, C.; Coppo, P.; Collins, R. F.; Turner, M. L.; Saiani, A.; Ulijn, R. V. Fmoc-diphenylalanine Self Assembles to a Hydrogel via a Novel Architecture Based on π–π Interlocked β-sheets. *Adv. Mater.* **2008**, *20*, 37–41.

(50) Ferry, J. D. Mechanical Properties of Substances of High Molecular Weight; Rigidities of Gelatin Gels; Dependence on Concentration, Temperature and Molecular Weight. *J. Am. Chem. Soc.* **1948**, *70*, 2244–2249.

(51) te Nijenhuis, K.; Dijkstra, H. Investigation of the Aging Process of a Polyvinyl Chloride Gel by the Measurement of its Dynamic Moduli. *Rheol Acta* **1975**, *14*, 71–84.

(52) Huang, X.; Terech, P.; Raghavan, S. R.; Weiss, R. G. Kinetics of 5α-Cholestan-3β-yl *N*-(2-Naphthyl)carbamate/*n*-Alkane Organogel Formation and its Influence on the Fibrillar Networks. *J. Am. Chem. Soc.* **2005**, *127*, 4336–4344.

(53) Collin, D.; Covis, R.; Allix, F.; Jamart-Grégoire, B.; Martinoty, P. Jamming Transition in Solutions Containing Organogelator Molecules of Amino-Acid Type: Rheological and Calorimetry Experiments. *Soft Matter* **2013**, *9*, 2947–2958.

(54) Terech, P.; Friol, S. Rheometry of an Androstanol Steroid Derivative Paramagnetic Organogel. Methodology for a Comparison with a Fatty Acid Organogel. *Tetrahedron* **2007**, *63*, 7366–7374.

(55) Nijenhuis, K. te. *Thermoreversible Networks: Viscoelastic Properties and Structure of Gels*; Advances in polymer science; Springer-Verlag, Berlin Heidelberg, Germany, 1997.

(56) Djabourov, M.; Nishinari, K.; Ross-Murphy, S. B. *Physical Gels from Biological and Synthetic Polymers*; Cambridge University Press, UK, 2013.
(57) Mandal, S. K.; Kar, T.; Das, P. K. Pristine Carbon-nanotube-included Supramolecular Hydrogels with Tunable Viscoelastic Properties. *Chem. Eur. J.* **2013**, *19*, 12486–12496.
(58) Al-Niaimi, F.; Chiang, N. Y. Z. Topical Vitamin C and the Skin: Mechanisms of Action and Clinical Applications. *J. Clin. Aesthet. Dermatol.* **2017**, *10*, 14–17.
(59) Du, J.; Cullen, J. J.; Buettner, G. R. Ascorbic Acid: Chemistry, Biology and the Treatment of Cancer. *Biochim. Biophys. Acta* **2012**, *1826*, 443–457.
(60) Teodorescu, F.; Oz, Y.; Quéniat, G.; Abderrahmani, A.; Foulon, C.; Lecoeur, M.; Sanyal, R.; Sanyal, A.; Boukherroub, R.; Szunerits, S. Photothermally Triggered On-demand Insulin Release from Reduced Graphene Oxide Modified Hydrogels. *J. Control. Release* **2017**, *246*, 164–173.
(61) Wu, J.; Chen, A.; Qin, M.; Huang, R.; Zhang, G.; Xue, B.; Wei, J.; Li, Y.; Cao, Y.; Wang, W. Hierarchical Construction of a Mechanically Stable Peptide-graphene Oxide Hybrid Hydrogel for Drug Delivery and Pulsatile Triggered Release *in vivo*. *Nanoscale* **2015**, *7*, 1655–1660.
(62) Li, B.; Zhang, L.; Zhang, Z.; Gao, R.; Li, H.; Dong, Z.; Wang, Q.; Zhou, Q.; Wang, Y. Physiologically Stable F127-GO Supramolecular Hydrogel with Sustained Drug Release Characteristic for Chemotherapy and Photothermal Therapy. *RSC Adv.* **2018**, *8*, 1693–1699.
(63) Liu, W.; Zhang, X.; Zhou, L.; Shang, L.; Su, Z. Reduced Graphene Oxide (rGO) Hybridized Hydrogel as a Near-infrared (NIR)/pH Dual-responsive Platform for Combined Chemo-photothermal Therapy. *J. Coll. Interf. Sci.* **2019**, *536*, 160–170.
(64) Samorì, C.; Sainz, R.; Ménard-Moyon, C.; Toma, F. M.; Venturelli, E.; Singh, P.; Ballestri, M.; Prato, M.; Bianco, A. Potentiometric Titration as a Straightforward Method to Assess the Number of Functional Groups on Shortened Carbon Nanotubes. *Carbon* **2010**, *48*, 2447–2454.
(65) Case, D. A.; Cerutti, D. S.; Cheatham, T. E.; Darden, T. A.; Duke, R. E.; Giese, T. J.; Gohlke, H.; Goetz, A. W.; Greene, D.; Homeyer, N.; Izadi, S.; Kovalenko, A.; Lee, T. S.; LeGrand, S.; Li, P.; Lin, C.; Liu, J.; Luchko, T.; Luo, R.; Mermelstein, D.; Merz, K. M.; Monard, G.; Nguyen, H.; Omelyan, I.; Onufriev, A.; Pan, F.; Qi, R.; Roe, D. R.; Roitberg, A.; Sagui, C.; Simmerling, C. L.; Botello-Smith, W. M.; Swails, J.; Walker, R. C.; Wang, J.; Wolf, R. M.; Wu, X.; Xiao, L.; York, D. M.; Kollman, P. A. Amber 2017, Reference Manual Principal Contributors to the Current Codes, University of California, San Francisco, 2017.

(66) Jorgensen, W. L.; Chandrasekhar, J.; Madura, J. D.; Impey, R. W.; Klein, M. L. Comparison of Simple Potential Functions for Simulating Liquid Water. *J. Chem. Phys.* **1983**, *79*, 926–935.

(67) Fox, T.; Kollman, P. A. Application of the RESP Methodology in the Parametrization of Organic Solvents. *J. Phys. Chem. B* **1998**, *102*, 8070–8079.

(68) Berendsen, H. J. C.; Postma, J. P. M.; van Gunsteren, W. F.; DiNola, A.; Haak, J. R. Molecular Dynamics with Coupling to an External Bath. *J. Chem. Phys.* **1984**, *81*, 3684–3690.

(69) Engler, E.; Wipff, G. *MD-DRAW Software. Display of Dynamic Structures from MD Simulations. In Crystallography of Supramolecular Compounds*, Kluwer Dordrecht.; Tsoucaris, G., Ed.; Nato Science Series C; 1996.

(70) Humphrey, W.; Dalke, A.; Schulten, K. VMD: Visual Molecular Dynamics. *J. Mol. Graph.* **1996**, *14*, 33–38.